Journal of Power Sources 195 (2010) 7578–7582

Contents lists available at ScienceDirect

Journal of Power Sources

journal homepage: www.elsevier.com/locate/jpowsour

Short communication

Direct immobilization of Pt–Ru alloy nanoparticles on nitrogen-doped carbon nanotubes with superior electrocatalytic performance

Shujuan Jiang[a], Lei Zhu[a], Yanwen Ma[a,b,*], Xizhang Wang[a], Jianguo Liu[c,d], Jianmin Zhu[d], Yining Fan[a], Zhigang Zou[c,d], Zheng Hu[a,*]

[a] Key Laboratory of Mesoscopic Chemistry of MOE and Jiangsu Provincial Lab for Nanotechnology, School of Chemistry and Chemical Engineering, Nanjing University, Nanjing 210093, China
[b] Jiangsu Key Lab for Organic Electronics and Information Displays, Institute of Advanced Materials, Nanjing University of Posts and Telecommunications, Nanjing 210003, China
[c] Department of Materials Science and Engineering, Nanjing University, Nanjing 210093, China
[d] National Laboratory of Solid State Microstructures, Nanjing University, Nanjing 210093, China

ARTICLE INFO

Article history:
Received 6 May 2010
Accepted 10 June 2010
Available online 18 June 2010

Keywords:
Direct methanol fuel cell
Electrocatalyst
Nitrogen-doped carbon nanotubes
Pt–Ru alloy nanoparticles
Methanol oxidation

ABSTRACT

Taking the advantage of the inherent chemical activity arisen from the nitrogen incorporation for nitrogen-doped carbon nanotubes (NCNTs), we have developed a facile strategy for the construction of binary Pt–Ru/NCNT electrocatalysts. Alloyed Pt–Ru nanoparticles have been directly immobilized onto the outer surface of NCNTs without pre-modification due to the nitrogen participation. The Pt–Ru nanoparticles have a high dispersion, a narrow size distribution of 2.5–3.5 nm and tunable chemical composition. These catalysts have been evaluated for methanol oxidation and show good stability and better CO tolerance than the monometallic Pt/NCNT catalyst due to the bifunctional and electronic effects. The Pt_5Ru_5/NCNT catalyst shows superior electrocatalytic performance to the commercial Pt_5Ru_5/C catalyst. The easy fabrication and excellent performance of the NCNT-based Pt–Ru alloy catalysts indicate their potential application in direct methanol fuel cells.

1. Introduction

Carbon-supported Pt–Ru alloy catalysts have received extensive attention due to their high activity for fuel oxidation and excellent tolerance toward CO-poisoning in proton exchange membrane fuel cells and direct methanol fuel cells (DMFCs) [1–7]. The performances of these catalysts strongly depend on the characteristics of Pt–Ru nanoparticles, the properties of carbon support, and the interaction between Pt–Ru and support [2–7]. Great efforts have been devoted to optimizing the catalyst by regulating the Pt–Ru nanoparticles for uniform size, high dispersion and controllable composition, or/and by exploring new carbon supports with large surface area, good stability and high electrical conductivity, e.g., carbon nanotubes (CNTs) [3–5,7–10]. Generally, due to the inert surface, CNTs should be chemically modified by acid oxidation [4,5,10] or noncovalent functionalization [5,11] before immobilizing the metal nanoparticles. By acid oxidation route, oxygen-containing functional groups are generated in the skeleton of CNTs but a large number of defects are unavoidably introduced, hence the CNTs' electrical conductivity and corrosion resistance are deteriorated [5]. Noncovalent functionalization could preserve the merits of CNTs but additional interlinkers of organic molecule or polymer may weaken the electron transport and binding between the catalytic active species and CNTs. To overcome these disadvantages, a potential strategy is doping CNTs with heteroatoms to generate chemically active sites in the CNTs, hereby the latter modification process could be much simplified. This strategy has been recently demonstrated in our report on the convenient immobilization of Pt-based nanoparticles onto the nitrogen-doped CNTs (NCNTs) without pre-modification due to the nitrogen participation [12,13]. In this study, we have extended this strategy to the construction of the highly important binary Pt–Ru alloy catalysts. The Pt–Ru nanoparticles in so-constructed Pt–Ru/NCNT catalysts have a high dispersion, a narrow size distribution and tunable chemical composition. The catalysts present quite good stability and better CO tolerance than the monometallic Pt/NCNT for methanol oxidation (MOR) due to the bifunctional and electronic effects and the Pt_5Ru_5/NCNT shows the best electrocatalytic performance superior to the commercial Pt_5Ru_5/C. The easy fabrication and excellent performance of the NCNT-based Pt–Ru alloy catalysts indicate their potential application in DMFCs.

* Corresponding authors. Tel.: +86 25 83686015; fax: +86 25 83686251.
E-mail addresses: iamywma@njupt.edu.cn (Y. Ma), zhenghu@nju.edu.cn (Z. Hu).

0378-7753/$ – see front matter © 2010 Elsevier B.V. All rights reserved.
doi:10.1016/j.jpowsour.2010.06.025

2. Experimental

2.1. Preparation and characterization of Pt–Ru/NCNT electrocatalysts

NCNTs with nitrogen content of 3–5% were synthesized at 650 °C by chemical vapor deposition as described in our previous paper [14]. The as-prepared NCNTs were refluxed in 6 M NaOH and 6 M HCl aqueous solution at 110 °C for 4 h in turn to remove the Al_2O_3 support and metal catalysts. The purified NCNTs were thoroughly washed with distilled water until the pH value of the filtrate reached 7, and then dried at 70 °C overnight for further study.

Alloyed Pt–Ru nanoparticles with Pt:Ru molar ratios from 8:2 to 1:9 were supported onto NCNTs by microwave-polyol method [15]. Briefly, 20 mg NCNTs was placed in 50 mL ethylene glycol (EG) and sonicated for 20 min to obtain a liquid suspension. The appropriate amount of H_2PtCl_6/EG and $RuCl_3$/EG solution were added to the suspension dropwise and magnetically stirred for 3 h, then 2 mL NaOH/EG solution (2 mol L^{-1}) was added into the above mixture. After stirring for 10 min, the mixture was put into a microwave oven (850 W) for 90 s irradiation, then filtrated. The solid sample was multi-washed with ethanol and finally vacuum-dried at room temperature, denoted as Pt_8Ru_2/NCNT, Pt_7Ru_3/NCNT, Pt_5Ru_5/NCNT, Pt_3Ru_7/NCNT, Pt_2Ru_8/NCNT and Pt_1Ru_9/NCNT according to the molar ratio of the used Pt and Ru precursors. Monometallic catalysts of Pt/NCNT and Ru/NCNT were also prepared by the similar method for comparison. The preset total metal loading for all the catalysts is 40.0%. The metal composition and loading for each catalyst were analyzed by inductively coupled plasma-atomic emission spectrometry (ICP-AES, JY38S).

The catalysts were characterized by X-ray diffraction (XRD, Philips X'pert Pro X-ray diffractometer with Cu Kα radiation of 1.5418 Å), transmission electron microscopy (TEM, JEOL-JEM-1005 at 100 kV), high-resolution TEM (HRTEM, JEM2010 at 200 kV), and X-ray photoelectron spectroscopy (XPS, Thermo ESCALAB 250).

2.2. Electrochemical analysis for the catalysts

The electrochemical performances of all the catalysts were evaluated in 20 mL electrolyte at 25 °C by a three-electrode cell connected to a CHI 660C workstation (CH Instrument, Inc.). A glassy carbon disk with an area of 0.071 cm^2 was used as a working electrode. Ag/AgCl and platinum wire served as reference and counter electrodes, respectively. Thin film electrode for each catalyst was prepared by the following procedure. Simply, the catalyst suspension with a concentration of 1.0 mg mL^{-1} was obtained by ultrasonic dispersion, and 20 μL suspension was then dropped onto the glassy carbon disk. After drying thoroughly, 0.5 μL of Nafion (Dupont, 5 wt%) was dropped onto the catalyst to act as binder and proton conductor, and the electrode was then dried at room temperature for 24 h for use [12,13].

CO-stripping experiments were conducted in 0.5 M H_2SO_4 solution which was purged with nitrogen for 30 min and then bubbled with CO gas (99.99%) for 15 min for CO adsorption on catalysts. The residual CO in the solution was subsequently removed by nitrogen purging for 40 min. The CO-stripping cyclic voltammetry (CV) curves were recorded within the potential between −0.25 and 1.0 V at a scan rate of 20 mV s^{-1}. The electrocatalytic activities of the catalysts for MOR were examined by CV curves in 0.5 M H_2SO_4 solution containing 1 M methanol in the potential range of 0–1.0 V at a scan rate of 50 mV s^{-1}. The steady-state chronoamperometry for the catalysts was also tested at the polarizing potential of 0.7 V under nitrogen protection. Considering the fuel consumption during the chronoamperometry test, 0.5 mL of 1 M CH_3OH/0.5 M H_2SO_4 solution was added into the testing electrolyte after 350–420 s. For comparison, the same electrochemical tests were also conducted for the commercial Pt_5Ru_5/C catalyst (E-TEK) as reference.

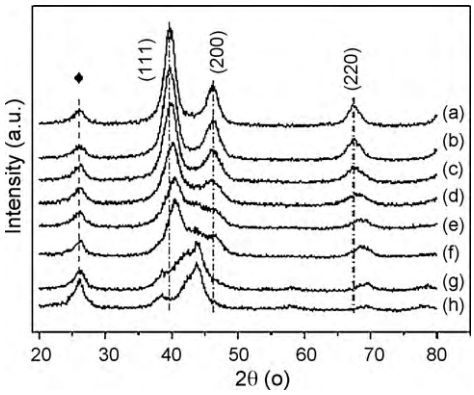

Fig. 1. XRD patterns of the catalysts. (a) Pt/NCNT; (b) Pt_8Ru_2/NCNT; (c) Pt_7Ru_3/NCNT; (d) Pt_5Ru_5/NCNT; (e) Pt_3Ru_7/NCNT; (f) Pt_2Ru_8/NCNT; (g) Pt_1Ru_9/NCNT and (h) Ru/NCNT.

3. Results and discussion

The metal loading and composition for the as-prepared catalysts were analyzed by ICP-AES (see Table S1 in supplementary material). These two parameters for each catalyst match well with the corresponding preset value and the Pt–Ru alloy composition could be regulated in a wide range. XRD patterns for the as-prepared Pt/NCNT, Pt–Ru/NCNT and Ru/NCNT catalysts are shown in Fig. 1. The diffraction peaks at 26.1° (marked with ♦) appear for all the samples, which arise from the (0 0 2) basal plane diffraction in the graphitic structure of the NCNTs. The Pt/NCNT catalyst (line a) shows three main diffraction peaks at 2θ of 39.8, 46.2 and 67.8°, corresponding to the (1 1 1), (2 0 0) and (2 2 0) plane of face-centered cubic (fcc) metallic Pt [12,13]. When the Pt metal on NCNTs are alloyed with Ru, the two main peaks for Pt(1 1 1) and (2 2 0) gradually up-shift with increasing the Ru/Pt ratio from 2/8 to 8/2 (lines b–f). This is caused by the shrinkage of Pt fcc lattice when Pt atoms are partially substituted by Ru atoms with smaller atomic radius [1]. Hence the Pt–Ru alloys in these samples take the Pt fcc-like structures. In contrast, the Pt–Ru alloy in Pt_1Ru_9/NCNT takes the hexagonal close-packed (hcp) structure similar to that of metal Ru due to the low Pt concentration. The XRD curve for Pt_1Ru_9/NCNT (lines g) is similar to that for Ru/NCNT (lines h) which displays four diffraction peaks at 38.4, 43.9, 57.9 and 69.1°, corresponding to (1 0 0), (1 0 1), (1 0 2) and (1 1 0) of hcp-Ru (JCPDS 06-0663). The evolution of the XRD curves for this series of Pt–Ru/NCNT catalysts is consistent with that of Pt–Ru bulk alloys [16]. This result indicates that the Pt and Ru in the Pt–Ru/NCNT catalysts are alloyed.

Fig. 2a–h shows the typical TEM images of the catalysts. For all the catalysts, the Pt–Ru alloy nanoparticles of 2.5–3.5 nm in sizes are homogeneously immobilized on the NCNTs with high dispersion. The catalysts are further characterized by HRTEM and the representative images for Pt_5Ru_5/NCNT catalyst are shown in Fig. 2i and j. The nanoparticles have spherical morphologies and tightly anchor on the surface of NCNTs. The lattice distance for ten layers of (1 1 1) planes is 2.26 nm as marked in Fig. 2j. In other words, the interplanar distance for Pt_5Ru_5 nanoparticles (0.226 nm) is slightly smaller than that of d_{111} for Pt (0.230 nm), suggesting the lattice shrinkage, in agreement with the XRD result.

The chemical states of the Pt and Ru species in the catalysts were analyzed by XPS as shown in Fig. 3 (see Figs. S1–3 in supplementary material). All the binding energies (E_b) are referenced to C 1s at 284.6 eV. The Pt 4f XPS spectrum for the monometallic Pt/NCNT catalyst presents two main peaks at about 71.4 and 74.6 eV

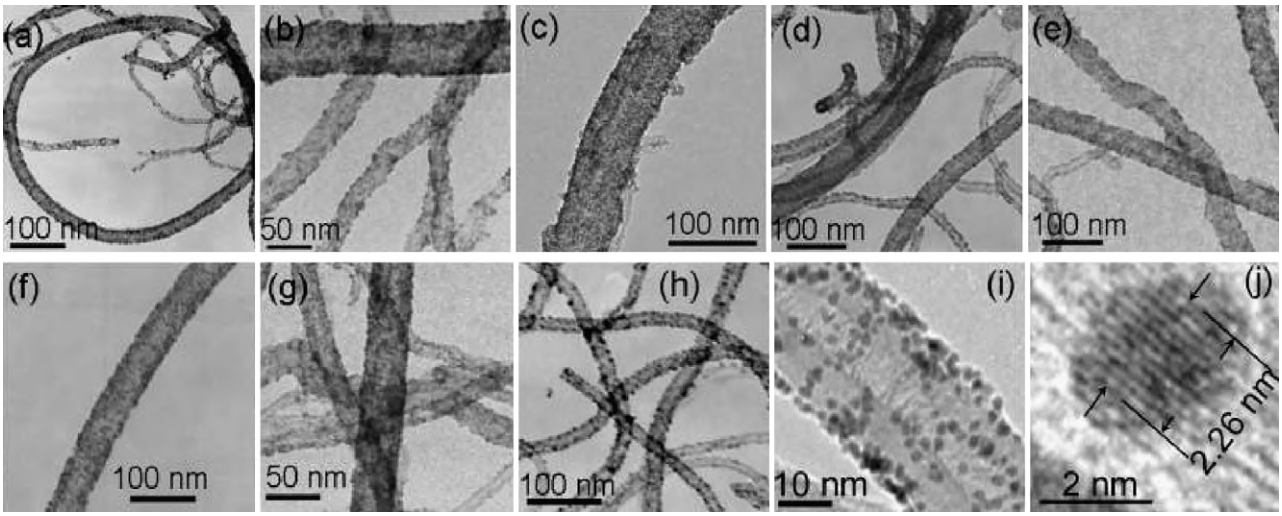

Fig. 2. Typical TEM and HRTEM images of the catalysts. (a) Pt/NCNT; (b) Pt_8Ru_2/NCNT; (c) Pt_7Ru_3/NCNT; (d, i, j) Pt_5Ru_5/NCNT; (e) Pt_3Ru_7/NCNT; (f) Pt_2Ru_8/NCNT; (g) Pt_1Ru_9/NCNT and (h) Ru/NCNT.

corresponding to the spin–orbit split doublet of Pt $4f_{7/2}$ and $4f_{5/2}$, respectively (Fig. 3a). In detail, three chemically different Pt entities could be identified, i.e. the predominant metallic Pt(0) and a little oxide species of Pt(II) and Pt(IV) (see Fig. S1 in supplementary material). The Ru $3p_{3/2}$ XPS spectrum for the monometallic Ru/NCNT catalyst presents one main peak at about 462 eV with a broad shoulder (Fig. 3b). This could also be identified into three different entities, i.e. the metallic Ru(0), RuO_2 and RuO_xH_y (see Fig. S2 in supplementary material). The chemical state of Pt or Ru in the bimetallic Pt–Ru/NCNT catalysts is similar to that of the monometallic ones, i.e. mainly in metallic state with a little oxide species (Fig. 3, Fig. S3 in supplementary material). It is seen that, with increasing the Ru/Pt ratio in Pt–Ru/NCNT, the signal intensity of the Pt 4f spectra decreases while that of the Ru 3p increases steadily as expected, indicating the tunable Pt/Ru atomic ratio (Fig. 3). Meanwhile, the E_b of Pt 4f gradually up-shifts by ~0.6 eV from the monometallic Pt/NCNT to Pt_1Ru_9/NCNT alloy catalyst (Fig. 3a), while the E_b for Ru $3p_{3/2}$ does not show observable shift with respect to that for Ru/NCNT. The enhanced E_b of Pt 4f for Pt–Ru/NCNT comes from the shift of d-band center towards higher E_b, which is caused by the lattice strain and charge transfer due to the Ru alloying [17–19]. Similar E_b changes for Pt and Ru were observed in Pt–Ru bulk alloys [17]. These results indicate that both the chemical composition and the electron state in the Pt–Ru/NCNT catalysts have been controllably regulated.

The preceding results suggest that, due to the intrinsic chemical activity, NCNT is an efficient support to anchor bimetallic Pt–Ru nanoparticles with narrow size distribution, high dispersion and tunable chemical composition. This provides an excellent platform for the exploration and optimization of new electrocatalysts. First, CO-stripping voltammetry were performed for all the catalysts to determine their electrochemical surface areas (ESAs) and to probe their capability of CO tolerance. The corresponding CV curve for each catalyst shows a single peak in the first scan (solid line) whereas the peak disappears in the second scan (dashed line), as presented in Fig. 4. This indicates that these peaks arise from the oxidation of CO adsorbed on the catalysts. After the complete removal of the adsorbed CO species via the first CV scan, the Pt sites in the Pt-containing catalysts were refreshed and could electrosorb hydrogen [20]. Hence hydrogen electrodesorption peaks around −0.2 V appear in the second CV scan curves. ESA for each catalyst obtained from the CO-stripping [21], together with the onset potential (E_{on}) and peak potential (E_{pk}) of the CO oxidation in Fig. 4, are listed in Table 1. It is seen that ESAs increase

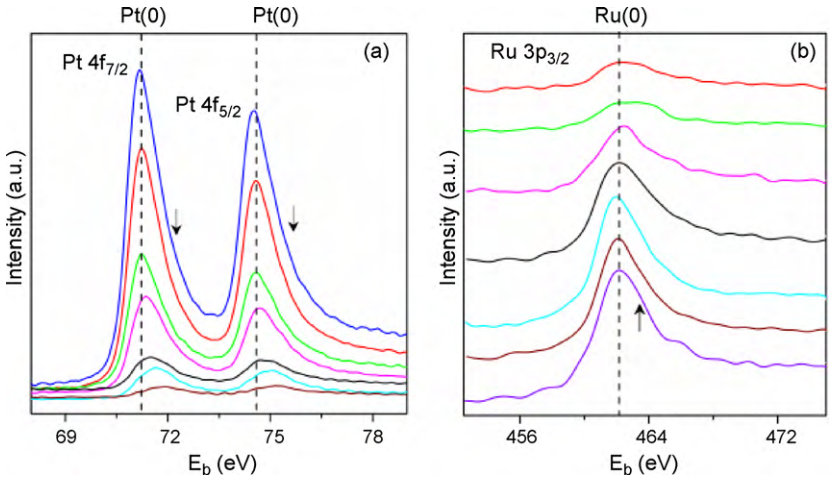

Fig. 3. Pt 4f and Ru $3p_{3/2}$ XPS spectra for Pt/NCNT, Pt–Ru/NCNT and Ru/NCNT catalysts. (a) The evolution of Pt 4f signal with decreasing Pt content from top (Pt/NCNT) to bottom (Pt_1Ru_9/NCNT). (b) The evolution of Ru $3p_{3/2}$ signal with increasing Ru content from top (Pt_8Ru_2/NCNT) to bottom (Ru/NCNT). The little broad shoulders marked with arrows indicate the coexistence of a little oxide species.

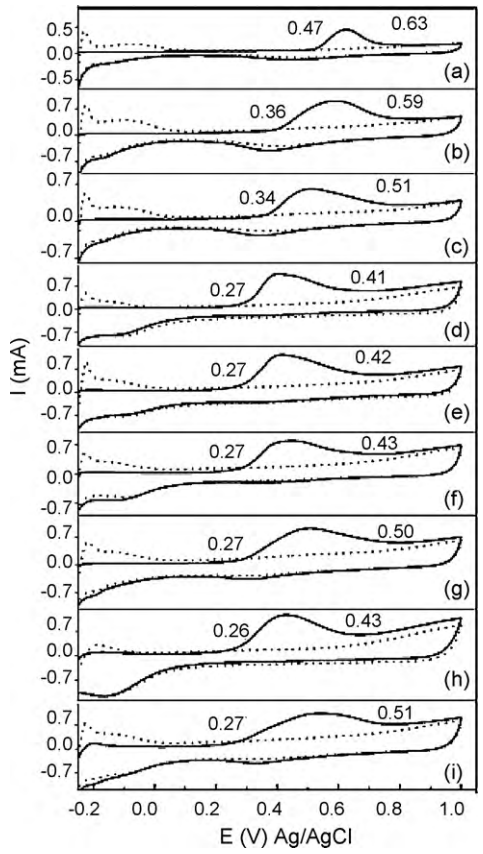

Fig. 4. CV curves of the first (solid line) and second (dashed line) CO-stripping scan in 0.5 M H_2SO_4 with a scan rate of 20 mV s^{-1} for the catalysts. (a) Pt/NCNT; (b) Pt_8Ru_2/NCNT; (c) Pt_7Ru_3/NCNT; (d) Pt_5Ru_5/NCNT; (e) Pt_3Ru_7/NCNT; (f) Pt_2Ru_8/NCNT; (g) Pt_1Ru_9/NCNT; (h) Ru/NCNT and (i) Pt_5Ru_5/C.

with increasing Ru content as anticipated due to the much lower atomic mass of Ru than Pt [22], and the more CO adsorption on each Ru than on each Pt [23]. Along with the change of ESA, the corresponding E_{on} and E_{pk} first negatively shift then change little with increasing Ru, giving the lowest E_{on} and E_{pk} for Pt_5Ru_5/NCNT. As known, the lower peak potential for CO oxidation means the higher tolerance of the catalyst to CO-poisoning [21]. Hence the binary alloyed Pt–Ru/NCNT catalysts, especially for those with the molar ratio of Ru/Pt over 1, exhibit enhanced tolerance to CO-poisoning in comparison with the monometallic Pt/NCNT catalyst, which could be mainly attributed to the bifunctional and electronic effects [16,24–26]. Compared with the commercial Pt_5Ru_5/C catalyst, the larger ESA and better tolerance to CO-poisoning for

Table 1
Electrochemical data obtained from CO-stripping and methanol oxidation for the as-prepared Pt/NCNT, Pt–Ru/NCNT and Ru/NCNT catalysts.

Samples	CO-stripping			MOR	
	E_{on} (V)	E_{pk} (V)	ESAs (m^2 g^{-1})	I_f (mA mg^{-1})	I_f/I_r
Pt/NCNT	0.47	0.63	66.0	159.2	1.1
Pt_8Ru_2/NCNT	0.36	0.59	93.7	201.1	1.2
Pt_7Ru_3/NCNT	0.34	0.51	100.5	222.0	1.3
Pt_5Ru_5/NCNT	0.27	0.41	124.4	290.6	3.2
Pt_3Ru_7/NCNT	0.27	0.42	139.4	94.7	2.7
Pt_2Ru_8/NCNT	0.27	0.43	143.1	61.7	2.4
Pt_1Ru_9/NCNT	0.27	0.50	159.2	53.7	3.8
Ru/NCNT	0.26	0.43	172.6	–	–
Pt_5Ru_5/C[a]	0.27	0.51	107.9	193.2	1.6

[a] Commercial Pt_5Ru_5/C catalyst with metal loading of 20% (E-TEK) was adopted to conduct the same electrochemical tests for reference.

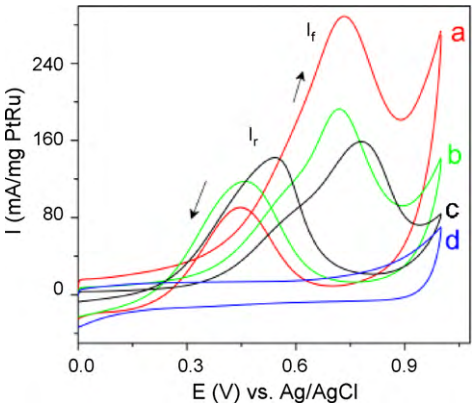

Fig. 5. Typical CV curves of MOR for the catalysts in 0.5 M H_2SO_4 and 1 M CH_3OH at the scan rate of 50 mV s^{-1}. (a) Pt_5Ru_5/NCNT; (b) Pt_5Ru_5/C; (c) Pt/NCNT and (d) Ru/NCNT. The CV curves for the other catalysts are shown in Fig. S4 in supplementary material.

Pt_5Ru_5/NCNT catalyst could be attributed to the higher dispersion and modified chemical state of the Pt species due to the nitrogen participation [21].

The electrochemical activities of the catalysts were tested by CV for MOR as the anodic half-cell reaction in DMFCs, and the corresponding CV curves are displayed in Fig. 5 and Fig. S4 in supplementary material. The maximum stable peak current density (I_f) corresponding to the mass activity for each catalyst appears around 0.72 V in the forward scan curve, which is attributed to the methanol oxidation. In the reverse scan, another oxidation peak (the peak current density is denoted as I_r) appears around 0.45 V, which is attributed to the oxidation of CO or CO-like species [27]. Ru/NCNT catalyst does not show response to MOR, similar to literature results [1]. Usually the high ratio of I_f/I_r suggests a better CO-poisoning tolerance [8,27]. The parameters I_f and I_f/I_r for each catalyst are also listed in Table 1. It is learnt that the catalytic activity follows the order of Pt_5Ru_5/NCNT > Pt_7Ru_3/NCNT > Pt_8Ru_2/NCNT > Pt_5Ru_5/C > Pt/NCNT > Pt_3Ru_7/NCNT > Pt_2Ru_8/NCNT > Pt_1Ru_9/NCNT, i.e. the Pt_5Ru_5/NCNT catalyst shows the highest activity. And the CO-poisoning tolerance follows the order of Pt_1Ru_9/NCNT > Pt_5Ru_5/NCNT > Pt_3Ru_7/NCNT > Pt_2Ru_8/NCNT > Pt_5Ru_5/C > Pt_7Ru_3/NCNT > Pt_8Ru_2/NCNT > Pt/NCNT, which is generally consistent with the changes of E_{on} and E_{pk} for CO oxidation. These results indicate that, alloying Pt with moderate Ru could simultaneously enhance the catalytic activity and CO-poisoning tolerance of the alloyed electrocatalysts, but excessive Ru would lead to the deterioration of the activity though with even better CO-poisoning tolerance. Hence appropriate amount of Ru is a key factor for optimizing the bifunctional and electronic effects to achieve the excellent performance of alloyed Pt–Ru/NCNT catalysts for MOR.

The long-term stabilities of the catalysts were examined and the steady-state chronoamperometries under a constant voltage of 0.7 V are shown in Fig. 6. After a transient period, the current densities for the catalysts follow the order of Pt_5Ru_5/NCNT > Pt_7Ru_3/NCNT ≈ Pt_8Ru_2/NCNT > Pt_5Ru_5/C > Pt/NCNT > Pt_3Ru_7/NCNT ≈ Pt_2Ru_8/NCNT ≈ Pt_1Ru_9/NCNT, and the Ru/NCNT catalysts shows a negligible signal. This is in agreement with the order of the catalytic activity obtained from the CV tests mentioned earlier. It is noticed that the current intensities decrease with scan proceeding especially for the catalysts with high activity such as Pt_5Ru_5/NCNT, Pt_7Ru_3/NCNT and Pt_8Ru_2/NCNT. This is mainly caused by the consumption of methanol as supported by the recovery test. When 0.5 mL CH_3OH/H_2SO_4 solution was added to the electrolyte after about 350–420 s testing, the current exhibits a sudden bounce. Pt_5Ru_5/NCNT catalyst presents the best recovery level, showing its highest activity for methanol oxidation. These

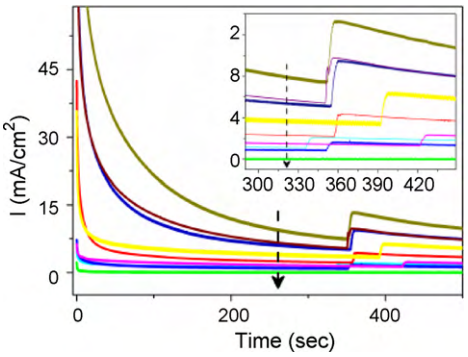

Fig. 6. The steady-state chronoamperometries for the catalysts at a constant voltage of 0.7 V vs. Ag/AgCl in 0.5 M H_2SO_4 electrolyte under nitrogen protection. From top to bottom: Pt_5Ru_5/NCNT, Pt_7Ru_3/NCNT, Pt_8Ru_2/NCNT, Pt_5Ru_5/C, Pt/NCNT, Pt_3Ru_7/NCNT, Pt_2Ru_8/NCNT, Pt_1Ru_9/NCNT and Ru/NCNT catalysts. During each test, 0.5 mL of 1 M methanol was added to the testing electrolyte after 350–420 s.

results indicate that, in addition to the large ESA and high tolerance to CO-poisoning, the optimum Pt_5Ru_5/NCNT catalyst also owns the competitive long-term stabilities to the commercial Pt_5Ru_5/C catalysts, suggesting its potential application in DMFCs.

4. Conclusion

A series of bimetallic alloyed Pt–Ru/NCNT electrocatalysts have been successfully constructed in a quite convenient way by taking the advantage of the inherent chemical activity of NCNTs. In addition to the high dispersion and narrow size distribution of 2.5–3.5 nm which are beneficial to electrocatalysis, the supported Pt–Ru alloyed nanoparticles could be regulated in a wide range of chemical composition so that the catalyst properties could be further optimized by bifunctional and electronic effects. Systematical evaluation on the electrocatalytic properties of these catalysts for methanol oxidation indicates the binary Pt–Ru/NCNT catalysts show quite good stability and better CO tolerance than the monometallic Pt/NCNT. The optimum Pt_5Ru_5/NCNT catalyst shows a superior electrocatalytic performance to the commercial Pt_5Ru_5/C catalyst. The easy fabrication and excellent performance of the binary Pt–Ru/NCNT catalysts indicate their potential application in DMFCs.

Acknowledgment

This work was jointly supported by NSFC (20833002, 20525312) and "973" Program (2007CB936300). We also acknowledge the support by the Program for Changjiang Scholars and Innovative Research Team in University (PCSIRT), as well as SRFGS of NU.

Appendix A. Supplementary data

Supplementary data associated with this article can be found, in the online version, at doi:10.1016/j.jpowsour.2010.06.025.

References

[1] S.H. Liu, W.Y. Yu, C.H. Chen, A.Y. Lo, B.J. Hwang, S.H. Chien, S.B. Liu, Chem. Mater. 20 (2008) 1622–1628.
[2] H.S. Liu, C.J. Song, L. Zhang, J.J. Zhang, H.J. Wang, D.P. Wilkinson, J. Power Sources 155 (2006) 95–110.
[3] Y.H. Lee, G. Lee, J.H. Shim, S. Hwang, J. Kwak, K. Lee, H. Song, J.T. Park, Chem. Mater. 18 (2006) 4209–4211.
[4] Y.J. Gu, W.T. Wong, Langmuir 22 (2006) 11447–114452.
[5] Y.L. Hsin, K.C. Hwang, C.T. Yeh, J. Am. Chem. Soc. 129 (2007) 9999–10010.
[6] C.K. Acharya, C.H. Turner, J. Phys. Chem. C 111 (2007) 14804–14812.
[7] W.Z. Li, X. Wang, Z.W. Chen, M. Waje, Y.S. Yan, J. Phys. Chem. B 110 (2006) 15353–15358.
[8] Z.L. Liu, X.Y. Ling, X.D. Su, J.Y. Lee, J. Phys. Chem. B 108 (2004) 8234–8240.
[9] R. Chetty, W. Xia, S. Kundu, M. Bron, T. Reinecke, W. Schuhmann, M. Muhler, Langmuir 25 (2009) 3853–3860.
[10] C.T. Hsieh, J.Y. Lin, S.Y. Yang, Physica E 41 (2009) 373–378.
[11] S.Y. Wang, X. Wang, S.P. Jiang, Langmuir 24 (2008) 10505–10512.
[12] B. Yue, Y.W. Ma, H.S. Tao, L.S. Yu, G.Q. Jian, X.Z. Wang, X.S. Wang, Y.N. Lu, Z. Hu, J. Mater. Chem. 18 (2008) 1747–1750.
[13] S.J. Jiang, Y.W. Ma, G.Q. Jian, H.S. Tao, X.Z. Wang, Y.N. Fan, Y.N. Lu, Z. Hu, Y. Chen, Adv. Mater. 21 (2009) 4953–4956.
[14] H. Chen, Y. Yang, Z. Hu, K.F. Huo, Y.W. Ma, Y. Chen, J. Phys. Chem. B 110 (2006) 16422–16427.
[15] S.H. Yang, W.H. Shin, J.W. Lee, H.S. Kim, J.K. Kang, Y.K. Kim, Appl. Phys. Lett. 90 (2007) 013103.
[16] H.A. Gasteiger, N. Markovic, P.N. Ross, E.J. Cairns, J. Phys. Chem. 97 (1993) 12020–12029.
[17] A. Lewera, W.P. Zhou, R. Hunger, W. Jaegermann, A. Wieckowski, S. Yockel, P.S. Bagus, Chem. Phys. Lett. 447 (2007) 39–43.
[18] M.A. Rigsby, W.P. Zhou, A. Lewera, H.T. Duong, P.S. Bagus, W. Jaegermann, R. Hunger, A. Wieckowski, J. Phys. Chem. C 112 (2008) 15595–15601.
[19] M. Wakisaka, S. Mitsui, Y. Hirose, K. Kawashima, H. Uchida, M. Watanabe, J. Phys. Chem. B 110 (2006) 23489–23496.
[20] R.J.K. Wiltshire, C.R. King, A. Rose, P.P. Wells, H. Davies, M.P. Hogarth, D. Thompsett, B. Theobald, F.W. Mosselmans, M. Roberts, A.E. Russell, Phys. Chem. Chem. Phys. 11 (2009) 2305–2313.
[21] Y.W. Ma, S.J. Jiang, G.Q. Jian, H.S. Tao, L.S. Yu, X.B. Wang, X.Z. Wang, J.M. Zhu, Z. Hu, Y. Chen, Energy Environ. Sci. 2 (2009) 224–229.
[22] Z. Jusys, J. Kaiser, R.J. Behm, Electrochim. Acta 47 (2002) 3693–3706.
[23] E.M. Crabb, M.K. Ravikumar, D. Thompsett, M. Hurford, A. Rosec, A.E. Russell, Phys. Chem. Chem. Phys. 6 (2004) 1792–1798.
[24] C. Bock, C. Paquet, M. Couillard, G.A. Botton, B.R. MacDougall, J. Am. Chem. Soc. 126 (2004) 8028–8037.
[25] C. Roth, N. Benker, R. Theissmann, R.J. Nichols, D.J. Schiffrin, Langmuir 24 (2008) 2191–2199.
[26] L. Giorgi, A. Pozio, C. Bracchini, R. Giorigi, S. Turtu, J. Appl. Electrochem. 31 (2001) 325–334.
[27] Z.C. Wang, Z.M. Ma, H.L. Li, Appl. Surf. Sci. 254 (2008) 6521–6526.